PROCEEDINGS of the
23rd International Congress on Acoustics

9 to 13 September 2019 in Aachen, Germany

Application of a computationally efficient coincidence detector model to simulate auditory brainstem neurons

Go ASHIDA[1,2]; Mathias DIETZ[1,3]; Jutta KRETZBERG[1,2]

[1] Cluster of Excellence "Hearing4all", University of Oldenburg, 26129 Oldenburg, Germany.

[2] Department of Neuroscience, University of Oldenburg, 26129 Oldenburg, Germany.

[3] Department of Medical Physics and Acoustics, University of Oldenburg, 26129 Oldenburg, Germany.

ABSTRACT

Computational modeling plays an important role in the investigation of acoustic information processing along the auditory system. Recent studies found that a relatively simple neuronal model, which produces action potentials depending on the count and timing of modeled synaptic inputs, can simulate a number of response features of auditory brainstem neurons, such as interaural time and intensity difference coding in the lateral superior olive. Here we review this simple coincidence detector model and discuss its possible applications to several other types of auditory neurons. Our application targets include principal neurons in the medial superior olive that change their number of action potentials according to interaural time differences and globular bushy cells in the anteroventral cochlear nucleus that show enhanced phase-locking to low frequency tones than auditory nerves. Because of its computational efficiency, the model is also suitable for large-scale simulations that typically include thousands of neurons to study, for example, across-frequency integration and the resulting perception of binaural sounds. Further modifications of the model for better biological plausibility, such as introducing an adaptive threshold, are also discussed.

Keywords: Physiological model, Auditory brainstem, Binaural neurons, Sound localization

1. INTRODUCTION

Modeling is a fundamental tool in theoretical studies of acoustic information processing in the brain. Models of binaural neurons, for example, allow us to investigate how these neurons integrate synaptic inputs originating from the two ears to detect binaural cues, such as the interaural time and level differences (ITDs/ILDs). A variety of models were created to simulate the functions of binaural neurons (reviewed in 1, 2).

Previous neuroscientific studies have revealed that mammals have specialized neuronal circuits in the brainstem to encode ITDs and ILDs (3). Ascending auditory nerve fibers project to spherical and globular bushy cells (SBCs/GBCs) in the anteroventral cochlear nucleus, which in turn innervate to several nuclei of the superior olivary complex (Figure 1A). SBCs send their excitatory inputs bilaterally to the medial superior olive (MSO) and ipsilaterally to the lateral superior olive (LSO). GBCs drive neurons in the contralateral medial nucleus of the trapezoid body (MNTB) that makes inhibitory projections to the ipsilateral MSO and LSO.

Neurophysiological recordings in vivo showed that phase-locking to low frequency tones (<1 kHz) in SBCs and GBCs is better than that of auditory nerves (4). The principal neurons of MSO vary its spiking output according to ITDs, by detecting the time difference of its ipsi- and contralateral excitatory synaptic inputs (3, 5). An LSO neuron, which is excited by ipsilateral sound and inhibited by contralateral sound, changes its spike rate depending on ILD. In addition, the output spike rate of a low-frequency LSO neuron is also affected by ITDs (6).

Depending on the purposes of modeling, neuron models can be simple or complex (7). Our previous study that compared different types of physiological models of LSO neurons revealed that both functional shot-noise models and more physiologically complex Hodgkin-Huxley-type models produce very similar results if they are calibrated with common criteria (8). Based on these results, we here aim to simulate the physiological functions of MSO, LSO and GBC using a computationally simple model. The model introduced in this study allows us to focus on the input-output relations of these neurons without considering their subneuronal, biophysical details.

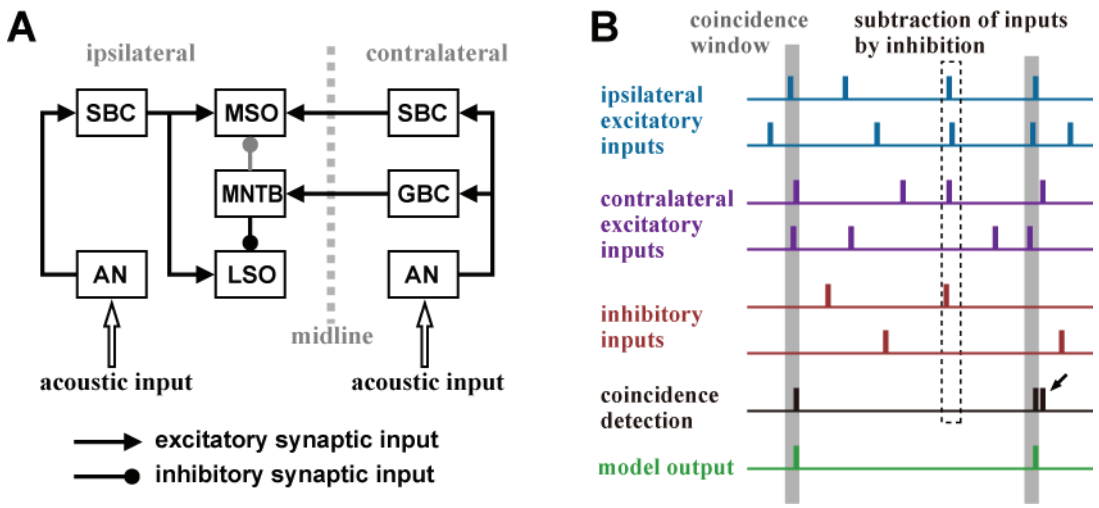

Figure 1 – **A**. Circuit diagram of the binaural circuit in the auditory brainstem. AN: auditory nerve; GBC: globular bushy cell; SBC: spherical bushy cell; MNTB: medial nucleus of the trapezoid body; MSO: medial superior olive; LSO: lateral superior olive. The inhibitory connection from MNTB to MSO (shown in gray) is not considered in the model here. **B**. Schematic description of the coincidence counting model. Each vertical bar represents a spike. Excitatory inputs (blue: ipsilateral; purple: contralateral) are summed in the coincidence window (vertical gray rectangles). If the number of input counts reaches the threshold (three in this example), an output spike is generated. The number of inhibitory inputs (red) occurring in the inhibition window (vertical dotted rectangle) is weighted and subtracted from the excitatory input counts. An output spike that is too close to a preceding spike is rejected by the refractory period (small black arrow).

2. METHODS

2.1 Coincidence Counting Model

The general structure of the *coincidence counting model* (8, 9, 10) is shown in Figure 1B. The model receives multiple excitatory inputs (possibly from various sources: blue and purple) and inhibitory inputs (red). A coincidence window (vertical gray band in Figure 1B) slides along the time axis. When the number of excitatory inputs in the coincidence window reaches or exceeds the threshold, an output spike is generated (green). If multiple threshold crossings occur within the refractory period, then only the first spike is counted, and the others are discarded (small arrow). Effects of inhibition were modeled as subtraction of excitatory inputs (or, equivalently, as an increase in threshold) for a certain time length (dotted vertical band). Detailed descriptions and analyses of the model were presented in (8, 9). We apply this model to MSO, LSO and GBC.

2.1.1 MSO Model

The MSO model receives ipsilateral and contralateral excitatory inputs. For simplicity, we here did not consider inhibitory inputs to MSO as in most previous studies (1, 10). To account for the non-zero peak position of the rate-ITD tuning curve, an internal (neuronal) delay between the ipsi- and contralateral inputs was used. Consequently, the parameters of the MSO model are the numbers of ipsi- and contralateral inputs, excitatory input threshold, length of the coincidence window, the length of the refractory period, and the size of the internal delay. Ipsilateral and contralateral inputs are assumed to share the same coincidence window and threshold. In this study, we did not consider monaural response of MSO neurons. Therefore, we did not use distinct monaural and binaural thresholds that were introduced in a previous study (10).

2.1.2 LSO Model

The LSO model receives ipsilateral excitatory inputs and contralateral inhibitory inputs, but not contralateral excitatory inputs (8, 9). To account for the non-zero trough position of the rate-ITD tuning curve, an internal (neuronal) delay between the ipsi- and contralateral inputs was used. The

parameters of the LSO model are the numbers of ipsi- and contralateral inputs, excitatory input threshold, length of the coincidence window, length of the inhibition window, amplitude of inhibition (i.e., how many excitatory inputs are cancelled by one inhibitory input), the length of the refractory period, and the size of the internal delay.

2.1.3 GBC Model

The GBC model receives only ipsilateral phase-locked excitatory inputs and no contralateral or inhibitory inputs. Its parameters are the numbers of inputs, excitatory input threshold, length of the coincidence window, and the length of the refractory period.

2.2 Phase-locked Input Model

We here consider only tone-evoked, sustained responses of MSO/LSO neurons and GBCs. To simulate phase-locked spike trains of their inputs, we used an inhomogeneous Poisson process combined with the von-Mises distribution function as its intensity function (9, 11). The degree of phase-locking, measured as vector strength (VS: 12), is mathematically related to the concentration parameter of the von-Mises distribution (11). The input model is thus characterized by the frequency, the average spiking rate, and the degree of phase-locking.

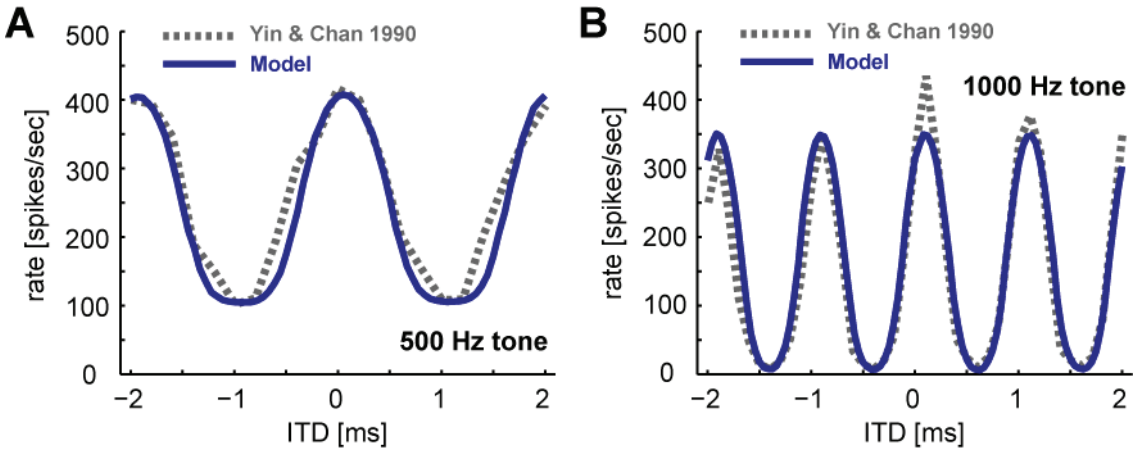

Figure 2 – Simulated ITD tuning of MSO. Model output (blue) is compared with experimental data (gray) by Yin and Chan (5). Parameters used are: (**A**) Frequency: 500 Hz; number of excitatory inputs: 4 (each side); excitatory input rate: 300 spikes/sec; VS of excitatory inputs: 0.9; binaural coincidence threshold: 2 inputs; coincidence window: 0.25 ms; refractory period: 1.6 ms; relative input delay: 0.06 ms (ipsilateral input lagging). (**B**) Frequency: 1000 Hz; number of excitatory inputs: 6 (each side); excitatory input rate: 300 spikes/sec; VS of excitatory inputs: 0.85; binaural coincidence threshold: 2 inputs; coincidence window: 0.08 ms; refractory period: 1.6 ms; relative input delay: 0.10 ms (ipsilateral input lagging).

3. RESULTS AND DISCUSSION

3.1 MSO Model - ITD Tuning

The model MSO neuron receives ipsi- and contralateral excitatory inputs arriving with time differences that depend on ITD and internal delay. Simultaneous arrivals of the inputs from the two sides result in a high output spike rate. The rate-ITD curves of the model (after parameter fitting) resembled those obtained in cat in vivo recordings (Figure 2). The peak position of the model tuning curve is determined by the internal delay, which is one of the model parameters. Without this delay, the model always produces a peak at zero ITD, because ipsi- and contralateral inputs are temporally symmetric with each other.

Previous *in vivo* recording studies indicated that inhibitory inputs from MNTB to MSO (3) as well as input history (13) affect the peak location of an ITD-tare tuning curve. Our minimalistic MSO

model, which does not explicitly simulate these effects, can nevertheless simulate the overall shape of the tuning curve (Figure 2), because the effect of peak shifting by various sources (of cochlear, axonal, synaptic, or neuronal origins) was simply incorporated into the relative delay of the inputs from the two sides.

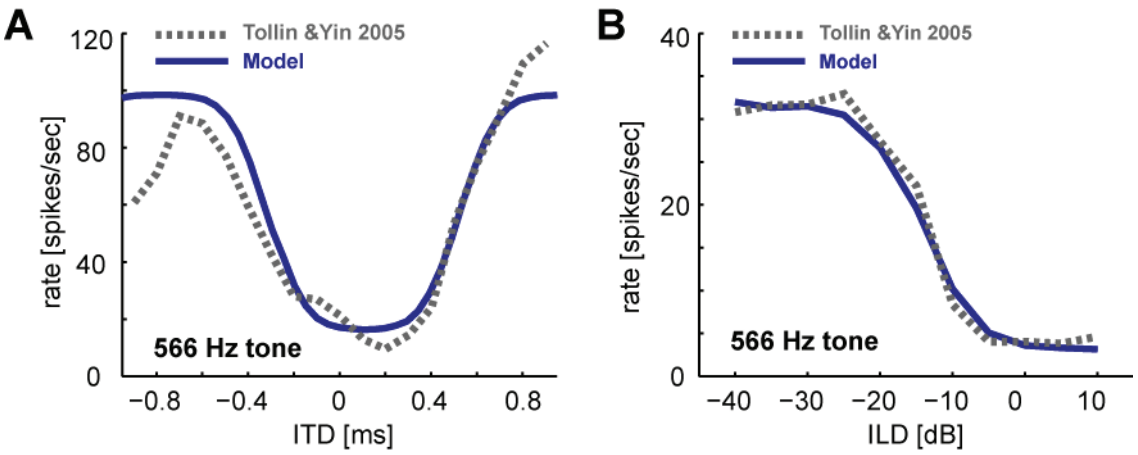

Figure 3 – Simulated binaural tuning of LSO: (A) ITD and (B) ILD. Model output (blue) is compared with experimental data (gray) by Tollin and Yin (6). Parameters used are: (A and B) Frequency: 566 Hz; number of excitatory inputs: 18; number of inhibitory inputs: 8; VS of excitatory inputs: 0.9; VS of inhibitory inputs: 0.9; coincidence threshold: 12 inputs; coincidence window: 0.4 ms; inhibition weight: 1 excitatory input; inhibition window: 0.8 ms; refractory period: 1.6 ms; relative input delay: 0.1 ms (contralateral input lagging). (A) Excitatory input rate: 300 spikes/sec; inhibitory input rate: 300 spikes/sec. (B) Excitatory (ipsilateral) input rate: 250 spikes/sec; ipsilateral level: 40 dB SPL. Inhibitory input rate was defined with a sigmoidal function of the sound intensity as $30 + 330/(1+\exp(-(L_c-30)/4))$ (spikes/sec), with L_c being the contralateral level in dB SPL.

3.2 LSO Model - ITD and ILD Tuning

The model LSO neuron receives ipsilateral excitatory inputs and contralateral inhibitory inputs. Because these inputs are phase-locked (if stimulated with low-frequency tones), the LSO model change its spike rate in not only an ILD- but also an ITD-dependent manner (Figure 3). Similar ITD-dependent spike-rate changes were observed in LSO neurons driven by binaural amplitude-modulated tones and were explained with (anti)coincidence detection between excitatory and inhibitory inputs (9).

Although the model ITD-tuning curve follows the overall trend of the ITD-dependence of the experimental data (Figure 3A), not all details could be simulated. First, the simulated ITD-tuning curve is more symmetric about the trough position than the experimental data, probably because synaptic input shapes are temporally symmetric in the model but not entirely so in the real system (8). Second, the two peaks of the cat data (at about -0.7 ms and +0.9 ms) are different in height (Figure 3A, gray), while the model predicted the same heights (Figure 3A, blue). We suspect that the asymmetry in the reference data is primary due to trail-to-trial variability, because LSO neurons driven by amplitude-modulated tones usually show more symmetric ITD-tuning curves (14).

Recent in vivo intracellular physiological recordings combined with anatomical characterizations found that neurons in LSO can be subdivided into several groups (15). Principal cells respond only at the onset of tonal stimuli, while non-principal cells respond in a more sustained manner, which was long (and wrongly) regarded as the canonical response pattern of representative LSO neurons. The model needs to be re-tuned to be able to simulate the onset-type responses of LSO principal neurons, which show only marginal dependence on ILDs to sustained tones.

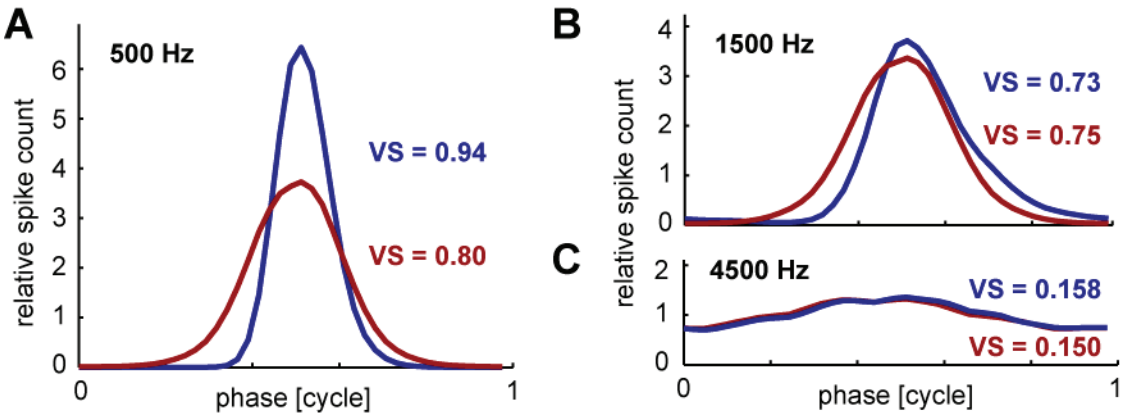

Figure 4 – Simulated phase-histograms at 500 Hz (A), 1500 Hz (B), and 4500 Hz (C). Inputs from AN are shown in red and the GBC outputs are shown in blue; corresponding VS values are also shown. Parameters used are: (A, B, and C) Number of excitatory inputs: 20; excitatory input rate: 250 spikes/sec; coincidence threshold: 5 inputs; coincidence window: 0.5 ms; refractory period: 1.4 ms.

3.3 GBC Model - Enhancement of Phase-locking

A GBC receives converging inputs from auditory nerves (16), which results in the improvement of phase-locking compared to auditory nerve inputs (17). This effect can be simulated in our model (Figure 4A). The enhancement of phase-locking is limited at low frequencies (typically 1 kHz or below) (Joris et al., 1994). Such frequency dependence is also seen in the model (Figure 4B), although the degradation of phase-locking at high frequency may not be as severe in the model as in experiments (Figure 4C).

Another prominent response characteristic of the GBC is the so-called "primary-like-with-notch" peristimulus time histogram, in which an onset peak of spiking activity is followed by a short pause and a gradual decrease (4, 18). However, since our goal here was to simulate the sustained activity of auditory neurons, we did not take the onset activity into account. To more faithfully simulate transient responses of GBCs, the model may need to include additional components such as an adapting threshold (19).

3.4 Limitations and Possible Modification of the Model

Despite its simplicity, the model we used can simulate fundamental temporal properties of MSO and LSO neurons and GBCs. The computational time required for the model was below 1% of that for a Hodgkin-Huxley-type model (8). This computational efficiency will allow us to calculate the responses of thousands of neurons simultaneously in future large-scale simulations, complementing the existing model framework using more complex models (20). Neurons in the cochlear nucleus neurons are physiologically and morphologically categorized into several groups (4, 21). Application of this simple model to neurons other than GBCs will be the topic of a future study.

Comparisons of the model outcome with experimental data obtained *in vivo* revealed that the simulated tuning curves are in general more symmetric than empirical tuning curves (Figure 3). In addition, the model GBC may represent better phase-locking than real neurons at high frequencies (Figure 4C). Several reasons may underlie these discrepancies. First, the modeled synaptic input is rectangular and reaches its maximum instantaneously at the onset, while real synaptic inputs of these neurons are temporally asymmetric and also subject to jitter (e.g., showing variability in amplitude and arrival time). To make the model more physiologically plausible, modifications of the input shape would be necessary but at the cost of reducing computational simplicity (7, 8).

4. CONCLUSIONS

In this work, we presented a simple coincidence counting model that can be applied to several types of auditory brainstem neurons, such as MSO, LSO and GBC. More specifically, ITD tuning of MSO and LSO, ILD tuning in LSO, and enhancement of phase-locking in GBCs were simulated. Because of its computational efficiency, the model can complement existing more complex models especially when the input-output function, but not the subneuronal biophysics, is the main focus of the simulation.

By modifying the shape of synaptic inputs, the model could gain a better physiological plausibility at the cost of partly losing its computational efficiency.

ACKNOWLEDGEMENTS

This work was supported by the Deutsche Forschungsgemeinschaft (DFG, German Research Foundation) under Germany's Excellence Strategy EXC 2177/1, Project ID 390895286 (GA and JK) and by the European Research Council (ERC) under the European Union's Horizon 2020 Research and Innovation Programme Grant Agreement no. 716800 (ERC Starting Grant to MD).

REFERENCES

1. Jennings TR, Colburn HS. Models of the superior olivary complex. In: Meddis R et al. (eds), Computational Models of the Auditory System (Springer Handbook of Auditory Research 35). New York, Springer.; 2010. p 65-96.
2. Dietz M, Ashida G. Computational models of binaural processing. In: Litovsky RY et al. (eds.), Binaural Hearing (Springer Handbook of Auditory Research). New York, Springer. (to appear)
3. Grothe B, Pecka M, McAlpine D. Mechanisms of sound localization in mammals. Physiol Rev. 2010; 90: 983-1012.
4. Joris PX, Carney LH, Smith PH, Yin TCT. Enhancement of neural synchronization in the anteroventral cochlear nucleus. I. Responses to tones at the characteristic frequency. J Neurophysiol. 1994; 71: 1022-1036.
5. Yin TCT, Chan JCK. Interaural time sensitivity in medial superior olive of cat. J Neurophysiol. 1990: 64: 465-488.
6. Tollin DJ, Yin TCT. Interaural phase and level difference sensitivity in low-frequency neurons in the lateral superior olive. J Neurosci. 2005; 25: 10648-10657.
7. Herz AVM, Gollisch T, Machens CK, Jaeger D. Modeling single-neuron dynamics and computations: a balance of detail and abstraction. Science. 2006; 314: 80-85.
8. Ashida G, Tollin DJ, Kretzberg J. Physiological models of the lateral superior olive. PLoS Comput Biol. 2017; 13: e1005903.
9. Ashida G, Kretzberg J, Tollin DJ. Roles for coincidence detection in coding amplitude-modulated sounds. PLoS Comput Biol. 2016; 12: e1004997.
10. Franken TP, Bremen P, Joris PX. Coincidence detection in the medial superior olive: mechanistic implications of an analysis of input spiking patterns. Front Neural Circuits. 2014; 8: 42.
11. Ashida G, Funabiki K, Carr CE. Theoretical foundations of the sound analog membrane potential that underlies coincidence detection in the barn owl. Front. Comput. Neurosci. 2013; 7: 151.
12. Goldberg JM, Brown PB. Response of binaural neurons of dog superior olivary complex to dichotic tonal stimuli: some physiological mechanisms of sound localization. J. Neurophysiol. 1969; 32: 613-636.
13. Franken TP, Roberts MT, Wei L, Golding NL, Joris PX. *In vivo* coincidence detection in mammalian sound localization generates phase delays. Nat Neurosci. 2015; 18: 444-452.
14. Joris PX, Yin TCT. Envelope coding in the lateral superior olive. I. Sensitivity to interaural time differences. J Neurophysiol. 1995; 73: 1043-1062.
15. Franken TP, Joris PX, Smith PH. Principal cells of the brainstem's interaural sound level detector are temporal differentiators rather than integrators. eLife. 2018; 7: e33854.
16. Spirou GA, Rager J, Manis PB. Convergence of auditory-nerve fiber projections onto globular bushy cells. Neuroscience. 2005; 136: 843-863.
17. Kuhlmann L, Burkitt AN, Paolini A, Clark G. Summation of spatiotemporal input patterns in leaky integrate-and-fire neurons: application to neurons in the cochlear nucleus receiving converging auditory nerve fiber input. J Comput Neurosci. 2002; 12: 55-73.
18. Smith PH, Rhode WS. Characterization of HRP-labeled globular bushy cells in the cat anteroventral cochlear nucleus. J Comp Neurol 1987; 266: 360-375.
19. Ashida G, Heinermann H, Kretzberg J. Computationally efficient physiological model of globular bushy cells. (submitted)
20. Manis PB, Campagnola L. A biophysical modelling platform of the cochlear nucleus and other auditory circuits: From channels to networks. Hear Res. 2018; 360: 76-91.
21. Blackburn CC, Sachs MB (1989) Classification of unit types in the anteroventral cochlear nucleus: PST histograms and regularity analysis. J Neurophysiol. 62: 1303-1329.